

Durham Research Online

Deposited in DRO:

19 February 2014

Version of attached file:

Accepted Version

Peer-review status of attached file:

Peer-reviewed

Citation for published item:

Shaw, A.M. and Hauri, E.H. and Behn, M.D. and Hilton, D.R. and Macpherson, C.G. and Sinton, J.M. (2012) 'Long-term preservation of slab signatures in the mantle inferred from hydrogen isotopes.', *Nature geoscience*, 5 (3). pp. 224-228.

Further information on publisher's website:

<http://dx.doi.org/10.1038/ngeo1406>

Publisher's copyright statement:

Additional information:

Use policy

The full-text may be used and/or reproduced, and given to third parties in any format or medium, without prior permission or charge, for personal research or study, educational, or not-for-profit purposes provided that:

- a full bibliographic reference is made to the original source
- a [link](#) is made to the metadata record in DRO
- the full-text is not changed in any way

The full-text must not be sold in any format or medium without the formal permission of the copyright holders.

Please consult the [full DRO policy](#) for further details.

Long-term preservation of slab signatures in the mantle inferred from hydrogen isotopes

A.M. Shaw^{1,*}, E.H. Hauri², M.D. Behn¹, D.R. Hilton³, C.G. Macpherson⁴ and J.M. Sinton⁵

¹ Department of Geology and Geophysics, Woods Hole Oceanographic Institution, Woods Hole MA, 02543 U.S.A.

² Department of Terrestrial Magnetism, Carnegie Institution of Washington, Washington DC, 20015 U.S.A.

³ Fluids & Volatiles Laboratory, Scripps Institution of Oceanography, UCSD, La Jolla CA, 92093-0244 U.S.A.

⁴ Department of Earth Sciences, Durham University, Durham, DH1 3LE, UK

⁵ Department of Geology and Geophysics, University of Hawai'i at Mānoa, Honolulu, HI, U.S.A.

Petrologic modeling of subduction zones indicates that water can be retained in down-going slabs to depths > 200 km¹ and seismic tomography studies show that many slabs are transported into the deep mantle. However, whether slab signatures can be preserved within the mantle depends on diffusion. Experimental studies of hydrogen (H) diffusion in mantle minerals^{1,2} suggest that H anomalies should equilibrate rapidly with ambient mantle at small scales, but homogenization at larger scales can only be achieved with relatively fast diffusivities. Based on existing H diffusivities, it was proposed that H isotope anomalies associated with material recycled from the surface would not be preserved³. Here, we challenge this notion based on new H and boron (B) isotope data from submarine glasses from the Manus back-arc basin. Specifically, we show that H isotopes are strongly correlated with geochemical tracers of subducted lithosphere, providing direct geochemical evidence for preservation of H isotope anomalies associated with an ancient slab in the mantle. Our geochemical data are consistent with calculations based on recent H diffusivity estimates in the upper mantle⁴ and transition zone⁵, and demonstrate that H isotope anomalies can persist in the mantle without suffering complete diffusive re-equilibration over timescales of 10⁸-10⁹ years.

*Corresponding Author: Alison M. Shaw, Dept. of Geology and Geophysics, Woods Hole Oceanographic Institution, 360 Woods Hole Road MS #22, Woods Hole, MA 02543, email: ashaw@whoi.edu, phone: 508-289-3775, fax: 508-457-2187.

The Manus back-arc basin is an ideal setting to study the behaviour of water and H isotopes in the mantle because most lavas are erupted at > 2000 m water depth (Fig. 1; Supplementary Table 1) minimizing the potentially fractionating effects of degassing, which can be significant in lavas erupted subaerially or into shallow water. Further, glasses from the basin have geochemical affinities ranging from incompatible element-depleted mid-ocean ridge basalt (MORB) to those showing variable imprints of subduction-related components⁶⁻¹¹, in addition to ³He/⁴He ratios up to 15R_A (ref⁸) and anomalously low δ¹⁸O (ref⁷), indicative of a superimposed plume. This geochemical variability allows for different source characteristics to be evaluated.

Water contents of Manus Basin glasses show a wide range of values from 0.09 wt% up to 1.6 wt% (Table 1; Fig. 2a). For comparison, MORBs, which tap the depleted upper mantle, generally have water contents < 0.4 wt%, while water in plume-derived ocean island basalts (OIBs) is highly variable (0.1-2 wt%). Prior studies of OIB glasses suggest that the primitive mantle produces water-rich basalt^{12,13}, whereas basalts derived from sources containing recycled subducted slabs are relatively dry^{14,15}. Hydrogen isotope (δD) values of Manus glasses display a strong, positive correlation with water content (Fig. 2a) and span a wide range from high, arc-like¹⁶ values of -33‰ to -126‰, significantly lower than those typical of MORB (-80 ± 10‰)¹⁷.

The high-water, high-δD values cannot be attributed to post-eruptive seawater contamination because Cl/K₂O ratios¹⁸ show no consistent pattern of enrichment in high δD glasses (Table 1). Therefore, elevated H₂O and δD values are most likely acquired by the mantle source from fluids derived from the actively subducting Solomon Sea Plate. Shaw et al.¹⁶ suggested that the high δD values of Mariana arc melt inclusions resulted from dehydration-induced fractionation of hydrous minerals in the slab. The high δD of water-rich Manus Basin

glasses is thus consistent with back-arc mantle that has been modified by dehydration-related fluids from actively subducting oceanic lithosphere.

The observed correlation between H isotopes and water contents can be attributed to either: (1) progressive lowering of δD and water content during degassing of water-rich back-arc magma, or (2) mixing between the back-arc component and an additional low-water, low- δD mantle source. Magmatic degassing of water can lower parental δD values, (e.g., ¹⁹), however, the Manus Basin glass data would require a vapour-melt fractionation factor (α) of 1.045 (Fig. 2a) – significantly higher than α values inferred from other locations or experiments ($\alpha = 1.012$ – 1.022)¹⁹. Furthermore, the most degassed Manus Basin glasses as measured by CO₂ contents and $\delta^{13}C$ values, have the highest δD values (Fig. 2b; Table 1)—a trend opposite to that expected for degassing, because the solubility of CO₂ in melts is significantly lower than that of H₂O¹⁰. Thus, we conclude that magmatic degassing has had a negligible effect on δD variations and that the observed correlations reflect mixing between a water-rich, high- δD subduction-related component and a separate component characterized by low water and low δD (see Supplementary Figure 1).

Two potential sources for the exceptionally low δD values in water-poor basalts are a relatively primitive mantle component or a recycled slab component. However, glasses from plume-related localities associated with relatively primitive mantle have δD values similar to MORB ($-80 \pm 10\%$)²⁰. In contrast, recycled oceanic lithosphere is predicted to have low δD because dehydration releases D-enriched fluids¹⁶. Melt inclusions from plume-related samples that show geochemical evidence for incorporation of dehydrated slabs have exceptionally low δD values (as low as -165%)²¹. Thus, we argue that the most likely source of the low δD endmember in the Manus Basin is a dehydrated slab component. This conclusion is supported

by boron isotope values, which are also fractionated during progressive dehydration of subducting crust²². $\delta^{11}\text{B}$ values of Manus Basin glasses are strongly correlated with δD values (Table 1; Fig. 2c) and trend towards lower values with decreasing B and water concentrations (Supplementary Table 2); consistent with dehydration-induced fractionation during subduction.

Trace element ratios can be used to further evaluate this conclusion because a dehydrated slab will also be depleted in fluid mobile elements (e.g., K, Ba, Pb, Rb, Sr, B), which are efficiently stripped out of sediments and oceanic lithosphere during subduction. Ba/La ratios, which are commonly used to track subduction fluids, are high in high- δD , arc-like glasses while low- δD samples have low Ba/La ratios (Fig. 2d), even lower than the global MORB average²³ and significantly lower than OIB²⁴. Ba/La values lower than MORB lend additional support to the notion that the low- δD source is derived from a dehydrated slab. The extent of dehydration can be evaluated using the $\text{H}_2\text{O}/\text{Ce}$ ratio¹⁴. $\text{H}_2\text{O}/\text{Ce}$ is strongly correlated with δD (Fig. 2e), where the lowest values correspond to low δD ; however, the lowest $\text{H}_2\text{O}/\text{Ce}$ ratio is higher than MORB source estimates (150 ± 10) and significantly higher than prior estimates of dehydrated recycled slabs (<100)¹⁴. This implies that either the recycled slab endmember has mixed with a higher $\text{H}_2\text{O}/\text{Ce}$ source (i.e., the pure low δD endmember has not been sampled), and/or slab dehydration is not as efficient as expected. Inefficient dehydration would suggest that significant amounts of water could be transferred to the deep mantle, thereby modifying the mantle's water budget over time.

Based on our new data, we favour a model in which the dehydrated slab signature originates from an ancient slab beneath the Manus Basin. It is unlikely that this component is associated with the actively subducting Solomon Sea Plate because the geochemical relationships are not correlated with the spatial distribution of samples—we do not observe lower Ba/La and lower δD

values with increasing distance from the trench (i.e., greater depths to slab; Fig. 1). Rather, we argue that the observed dehydrated slab signature is associated with a remnant slab from a prior subduction event. This is consistent with seismic tomography, which shows a broad fast seismic velocity anomaly between 800 and 1000 km beneath the Manus Basin (anomaly A8 in Fig. 1) that could be a remnant of Cretaceous subduction²⁵. We note that the low- δD glasses also have very low contents of incompatible trace elements and, likewise, do not have major element compositions consistent with a crustal component in their source¹¹. This may indicate that the remnant subducted component giving rise to the subduction-related isotopic characteristics is subducted lithospheric mantle and/or lower crustal cumulates, which would be consistent with the low $\delta^{18}O$ value inferred for this endmember⁷. Finally, neon isotopes of the Manus Basin glasses⁹ are strongly nucleogenic (having a high $^{21}Ne/^{22}Ne$ ratio for a given $^{20}Ne/^{22}Ne$ ratio), inconsistent with derivation from relatively primitive mantle. Our interpretation of the neon isotope characteristics is that a degassed source – in this case, a subducted slab – has grown in a nucleogenic Ne isotope signature over time. The time required to grow in the nucleogenic signature depends on the amount of Ne degassed from the slab during subduction and the U+Th concentration of the slab⁹. For example, a MORB-like source that had lost 98% of its neon would grow in the requisite Ne isotope signature within ~100 Ma.

To determine whether a dehydrated slab signature could be preserved in the mantle, we evaluate the timescale over which diffusion would obscure H isotope signatures acquired during subduction. We calculated diffusion as a function of time for water and δD using experimentally-determined H diffusion rates in olivine⁴ at upper mantle conditions (Fig. 3). We assume a 10-km thick slab with an initial water content of 0.5 wt% (ref²⁶), a δD value = -200‰ (ref¹⁶) and mantle temperature of 1600°C. The thickness assumes that the pervasively hydrated

portion of the slab includes 6 km of crust and the uppermost 4 km of the mantle²⁶. This modeling finds that anomalies in both water concentrations and H isotopes can persist over relatively long time-scales. For example, 25% of the initial anomaly is preserved for 0.5 and > 1 billion years for water concentrations and H isotopes, respectively (Fig. 3). Differences in the initial slab water content and mantle temperature will influence these calculations (Fig. 3c & d) but, in all cases, the Manus Basin δD anomaly (-126‰) would be preserved for at least ~200 Myr. Finally, although there are few data constraining H diffusivities in transition zone and lower mantle minerals, experimental data for wadsleyite indicate diffusivities similar to that of olivine at 1600°C (ref⁵). Variations in electrical conductivity across the Pacific basin also imply that H diffusion must be sufficiently slow such that water heterogeneities can persist in the transition zone⁵.

Transport of remnant slab signatures to the surface is often attributed to entrainment in buoyant mantle plumes ascending from the deep mantle. Manus Basin submarine glasses have high $^3\text{He}/^4\text{He}$ ratios⁸ (up to $15R_A$, as compared to MORB, which is typically $8 \pm 1 R_A$), the classic geochemical interpretation of which is derivation from a relatively undegassed mantle plume. The strong correlation of $^3\text{He}/^4\text{He}$ ratios with δD values (Fig. 2f) would imply that the plume and remnant slab components were well mixed prior to eruption.

Alternatively, ambient mantle flow associated with back-arc spreading could transport the slab signature to the surface, but this would require the ancient slab, itself, to be the source of high- $^3\text{He}/^4\text{He}$. Recent experimental studies have suggested that high $^3\text{He}/^4\text{He}$ could develop in residues depleted in U and Th by ancient melting events²⁷. However, such residues would also be very poor in He, due to its incompatibility. This is inconsistent with the relatively high He concentrations of Manus Basin high $^3\text{He}/^4\text{He}$ glasses⁸. Furthermore, time evolution models of

$^3\text{He}/^4\text{He}$ in a U- and Th-depleted, MORB mantle peridotite slab²⁸, would require more than 1 billion years isolation to yield the highest $^3\text{He}/^4\text{He}$ reported in Manus Basin glass (15R_A). If the observed δD anomalies are associated with a slab of Cretaceous age²⁵, then the high $^3\text{He}/^4\text{He}$ could not have been derived from the slab itself. Thus, we favour a scenario where the geochemical signatures result from mixing between a slab and an upwelling mantle plume.

Our finding that water and H isotope anomalies generated in slabs during subduction can be preserved over long time scales (10^8 – 10^9 years) has important implications for how water and other geochemical signatures are preserved in the mantle and ultimately recycled to the surface. For example, significant amounts of water are thought to be stripped from subducting slabs as they descend through the transition zone²⁹. However, if the geochemical anomalies recorded in the Manus Basin are indeed associated with the seismic anomaly imaged beneath the transition zone, these data indicate that H isotope anomalies are preserved after transit to the lower mantle. Given that hydrogen should diffuse faster than other chemical species, our results show that remnant slabs in the lower mantle can preserve their chemical signatures, supporting the longstanding view that these signatures may later be observed in OIBs.

Acknowledgements

We thank A. Gurenko (WHOI) and J. Wang (CIW) for assistance with the ion probe measurements. Funding was provided by the NSF (grant EAR-0646694) and the WHOI Deep Ocean Exploration Institute.

Author Contributions

167 JS provided the samples, AS & EH collected the geochemical data, MB & AS performed the
168 diffusion calculations, all authors contributed to the interpretation of the data, and AS took the
169 lead in preparing the manuscript with input from the other authors.
170

Methods Summary:

We measured major elements, trace elements, and major volatile concentrations (H_2O , CO_2 , F, S, and Cl) on 23 submarine glass samples from the Manus back-arc Basin. Subsets of these samples were selected for H and B isotope analyses. Glasses were mounted in indium metal (volatile blanks are significantly lower for indium mounts than for epoxy) and polished for ion and electron probe analyses. All analyses were carried out on the same individual glass fragments. Major elements were measured on the glasses with a JEOL Superprobe at the Geophysical Laboratory using a 15 kV accelerating voltage, a 10 nA beam intensity, and a spot size of 10 μm . Trace elements were measured using the Cameca 6f ion microprobe at the Carnegie Institution of Washington, using a 14–16 nA beam of O^- with a 15–20 μm spot and detection of positive secondary ions with a nominal acceleration voltage of 10 kV. Energy filtering was employed (-75 ± 25 eV) and the calibration checked using NBSSRM and MPI-DING glasses. Trace element detection limits were measured using Herasil glass, and are very low (~ 50 ppb for Sr and Ba; ~ 20 ppb for Hf and Rare Earth Elements (REEs); ~ 5 ppb for Nb). Combined accuracy and precision is 7% (2σ). Analytical reproducibility on separate chips of the same glass is typically 2–3% (2σ). Hydrogen isotopes and volatile abundances were measured using the 6f Cameca ion probe at the Carnegie Institution of Washington following established techniques¹⁶. All hydrogen isotope data have been corrected for fractionations associated with matrix effects (known to vary with host compositions) and instrument mass fractionation encountered during analyses — see²⁰. Combined accuracy and precision is $\sim 10\%$ (2σ). B isotopes were measured on WHOI’s 1280 ion microprobe using a new suite of natural glass standards along with synthetic NBS standard glasses, for calibration. The analyses were carried out using a 40 nA O^- beam rastered over a 30 μm area.

Figure Legends:

Figure 1. (Top) Regional map illustrating location of Manus Basin study area (black box). Red curves denote upper (solid) and lower (dashed) mantle seismic anomalies, labeled A3, A5 and A8 (ref²⁵). Inset shows an expanded view of the study area, with MORB (circle), back-arc basin (triangle), and arc (diamond) type samples shaded by their δD value ($\delta D = 1000 \times [(D/H)_{\text{sample}} - (D/H)_{\text{SMOW}}]/(D/H)_{\text{SMOW}}$, where SMOW is standard mean ocean water with $\delta D = 0\text{‰}$). Black symbols were not analyzed for δD . (Bottom) Vertical cross section through the tomography model of *Hall & Spakman*²⁵. The location of the cross section is shown by the solid black line X-X' in the top panel.

Figure 2. Hydrogen isotope ratios (δD) of Manus Basin glasses versus (a) H_2O , (b) CO_2 , (c) $\delta^{11}B$, (d) Ba/La , (e) H_2O/Ce and (f) $^3He/^4He$ (R/R_A). Back-arc basin basalts (BABBs), MORBs and arc samples³⁰ are shown as open triangles, filled blue circles, and grey diamonds, respectively. The dashed line in (a) shows the degassing trend that best fits the data ($\alpha = 1.045$). In (c) we show the mixing trend (solid line) between an arc source having $\delta D = -35\text{‰}$, $\delta^{11}B = 10\text{‰}$, 10 ppm B and 1.5 wt% water and a plume or recycled slab component with $\delta D = -130\text{‰}$, $\delta^{11}B = -10\text{‰}$, 2 ppm B and 0.1 wt% water. The ticks represent the proportion of the arc component.

Figure 3. Modeled diffusion profiles for water and δD as a function of distance and time. Using the model parameters described in the text, we show the distance that (A) water and (B) δD anomalies migrate over time. The white contour line shows where the anomaly has reached 25% of its original size. Maximum values of (C) water and (D) δD anomalies versus time are shown

219 assuming initial slab water contents of 500 ppm (blue) and 300 ppm (red) for mantle
220 temperatures of 1400°C (dashed curves) and 1600°C (solid curves). Even in the case with the
221 fastest diffusion (300 ppm initial, 1600°C), the minimum δD value of the Manus samples would
222 be retained for ~ 200 Myr.

223

224

References

- 1 Mackwell, S. J. & Kohlstedt, D. L. Diffusion of hydrogen in olivine - implications for water in the mantle. *J. Geophys. Res.-Solid Earth and Planets* **95**, 5079-5088 (1990).
- 2 Portnyagin, M., Almeev, R., Matveev, S. & Holtz, F. Experimental evidence for rapid water exchange between melt inclusions in olivine and host magma. *Earth Planet. Sci. Lett.* **272**, 541–552 (2008).
- 3 Workman, R. K., Hauri, E. H., Hart, S. R., Wang, J. & Blusztajn, J. Volatile and trace elements in basaltic glasses from Samoa: Implications for water distribution in the mantle. *Earth Planet. Sci. Lett.* **241**, 932-951 (2007).
- 4 Demouchy, S. & Mackwell, S. Mechanisms of hydrogen incorporation and diffusion in iron-bearing olivine. *Physics and Chemistry of Minerals* **33**, 347-355 (2006).
- 5 Hae, R., Ohtani, E., Kubo, T., Koyama, T. & Utada, H. Hydrogen diffusivity in wadsleyite and water distribution in the mantle transition zone. *Earth Planet. Sci. Lett.* **243**, 141-148 (2006).
- 6 Beier, C., Turner, S. P., Sinton, J. M. & Gill, J. B. Influence of subducted components on back-arc melting dynamics in the Manus Basin. *Geochem. Geophys. Geosys.* **11** doi:Q0ac0310.1029/2010gc003037 (2010).
- 7 Macpherson, C. G., Hilton, D. R., Matthey, D. P. & Sinton, J. M. Evidence for an ^{18}O -depleted mantle plume from contrasting $^{18}\text{O}/^{16}\text{O}$ ratios of back-arc lavas from the Manus Basin and Mariana Trough. *Earth Planet. Sci. Lett.* **176**, 171-183 (2000).
- 8 Macpherson, C. G., Hilton, D. R., Sinton, J. M., Poreda, R. J. & Craig, H. High $^3\text{He}/^4\text{He}$ ratios in the Manus backarc basin: Implications for mantle mixing and the origin of plumes in the western Pacific Ocean. *Geology* **26**, 1007-1010 (1998).
- 9 Shaw, A. M., Hilton, D. R., Macpherson, C. G. & Sinton, J. M. Nucleogenic neon in high $^3\text{He}/^4\text{He}$ lavas from the Manus back-arc basin: a new perspective on He-Ne decoupling. *Earth Planet. Sci. Lett.* **194**, 53-66 (2001).
- 10 Shaw, A. M., Hilton, D. R., Macpherson, C. G. & Sinton, J. M. The CO_2 -He-Ar- H_2O systematics of the Manus back-arc basin: Resolving source composition from degassing and contamination effects. *Geochim. Cosmochim. Acta* **68**, 1837-1856 (2004).
- 11 Sinton, J. M., Ford, L. L., Chappell, B. & McCulloch, M. T. Magma genesis and mantle heterogeneity in the Manus back-arc basin, Papua New Guinea. *J Petrol* **44**, 159-195 (2003).
- 12 Dixon, J. E., Clague, D. A., Wallace, P. & Poreda, R. Volatiles in alkalic basalts from the North Arch volcanic field, Hawaii: Extensive degassing of deep submarine-erupted alkalic series lavas. *J. Petrol.* **38**, 911-939 (1997).
- 13 Poreda, R., Schilling, J. G. & Craig, H. Helium and hydrogen isotopes in ocean-ridge basalts north and south of Iceland. *Earth Planet. Sci. Lett.* **78**, 1-17 (1986).
- 14 Dixon, J. E., Leist, L., Langmuir, C. & Schilling, J.-G. Recycled dehydrated lithosphere observed in plume-influenced mid-ocean-ridge basalt. *Nature* **420**, 385-389 (2002).
- 15 Jambon, A. & Zimmermann, J. L. Water in Oceanic Basalts - Evidence For Dehydration of Recycled Crust. *Earth Planet. Sci. Lett.* **101**, 323-331 (1990).
- 16 Shaw, A. M., Hauri, E. H., Fischer, T. P., Hilton, D. R. & Kelley, K. A. Hydrogen isotopes in Mariana arc melt inclusions: Implications for subduction dehydration and the deep-Earth water cycle. *Earth Planet. Sci. Lett.* **275**, 138-145 (2008).

- 17 Poreda, R. Helium -3 and deuterium in back-arc basalts; Lau Basin and the Mariana Trough. *Earth Planet. Sci. Lett.* **73**, 244-254 (1985).
- 18 Kent, A. J. R., Norman, M. D., Hutcheon, I. D. & Stolper, E. M. Assimilation of seawater-derived components in an oceanic volcano: evidence from matrix glasses and glass inclusions from Loihi seamount, Hawaii. *Chem. Geol.* **156**, 299-319 (1999).
- 19 Newman, S., Epstein, S. & Stolper, E. Water, Carbon-Dioxide, and Hydrogen Isotopes in Glasses from the Ca 1340 A.D. Eruption of the Mono Craters, California - Constraints on Degassing Phenomena and Initial Volatile Content. *J. Volcanol. Geotherm. Res.* **35**, 75-96 (1988).
- 20 Hauri, E. H., et al. Matrix effects in hydrogen isotope analysis of silicate glasses by SIMS. *Chem. Geol.* **235**, 352-365 (2006).
- 21 Hauri, E. SIMS analysis of volatiles in silicate glasses, 2: isotopes and abundances in Hawaiian melt inclusions. *Chem. Geol.* **183**, 115-141 (2002).
- 22 Marschall, H. R., Altherr, R. & Rupke, L. Squeezing out the slab - modelling the release of Li, Be and B during progressive high-pressure metamorphism. *Chem Geol* **239**, 323-335 (2007).
- 23 Su, Y. & Langmuir, C. H. Global MORB chemistry compilation at the segment scale. *petdb*.
- 24 Hofmann, A. W. in *The Mantle and Core Vol. 2 Treatises on Geochemistry* (ed R. W. Carlson) 61-101 (Elsevier, 2005).
- 25 Hall, R. & Spakman, W. Subducted slabs beneath the eastern Indonesia-Tonga region: insights from tomography. *Earth Planet. Sci. Lett.* **201**, 321-336 (2002).
- 26 Hacker, B. R. H₂O subduction beyond arcs. *Geochem. Geophys. Geosys.* **9**, Q03001, doi:03010.01029/02007GC001707 (2008).
- 27 Parman, S. W., Kurz, M. D., Hart, S. R. & Grove, T. L. Helium solubility in olivine and implications for high He-3/He-4 in ocean island basalts. *Nature* **437**, 1140-1143, (2005).
- 28 Jackson, M. G., Kurz, M. D., Hart, S. R. & Workman, R. K. New Samoan lavas from Ofu Island reveal a hemispherically heterogeneous high He-3/He-4 mantle. *Earth Planet. Sci. Lett.* **264**, 360-374 (2007).
- 29 Bercovici, D. The generation of plate tectonics from mantle convection. *Earth Planet. Sci. Lett.* **205**, 107-121 (2003).
- 30 Marty, B., Sano, Y. & France-Lanord, C. Water-saturated oceanic lavas from the Manus Basin: volatile behaviour during assimilation-fractional crystallisation-degassing (AFCD). *J. Volcanol. Geotherm. Res.* **108**, 1-10 (2001).

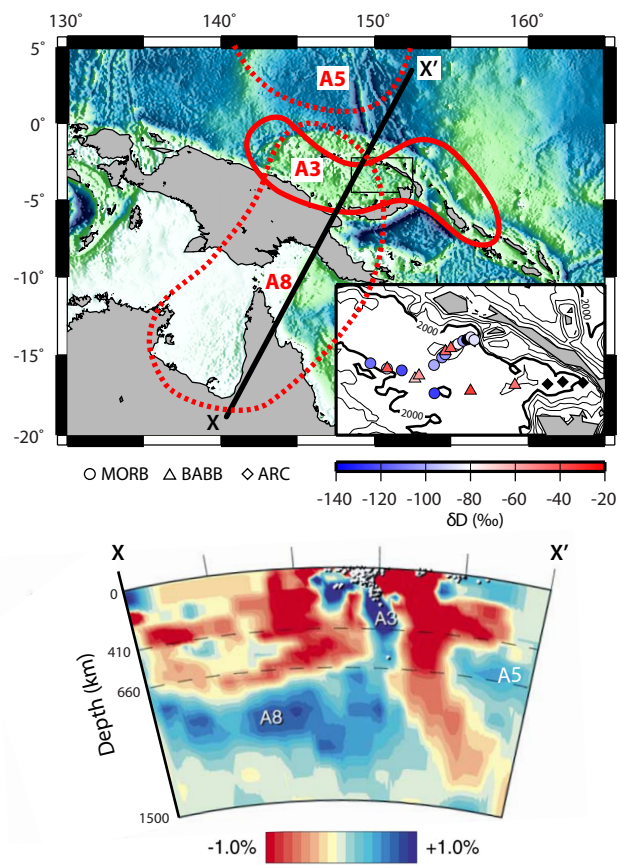


Figure 1

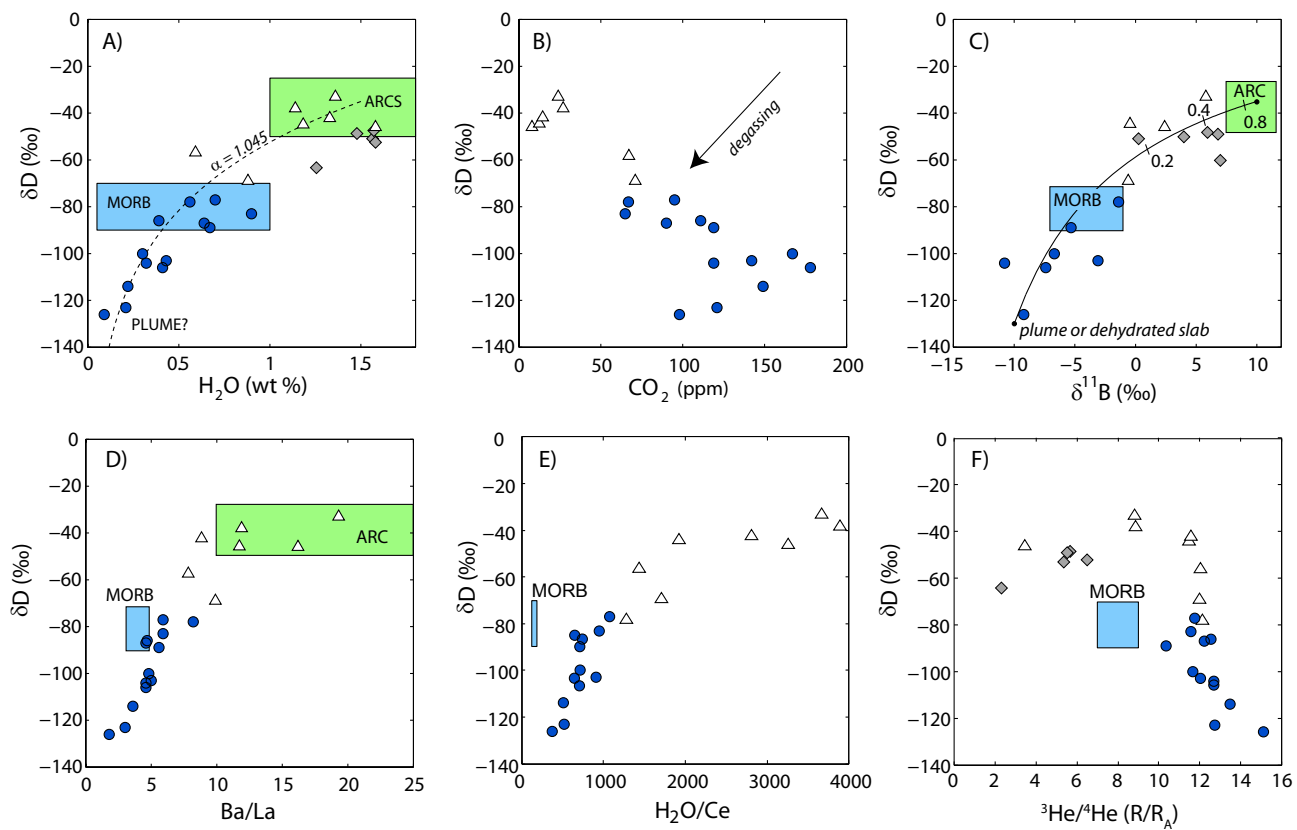


Figure 2

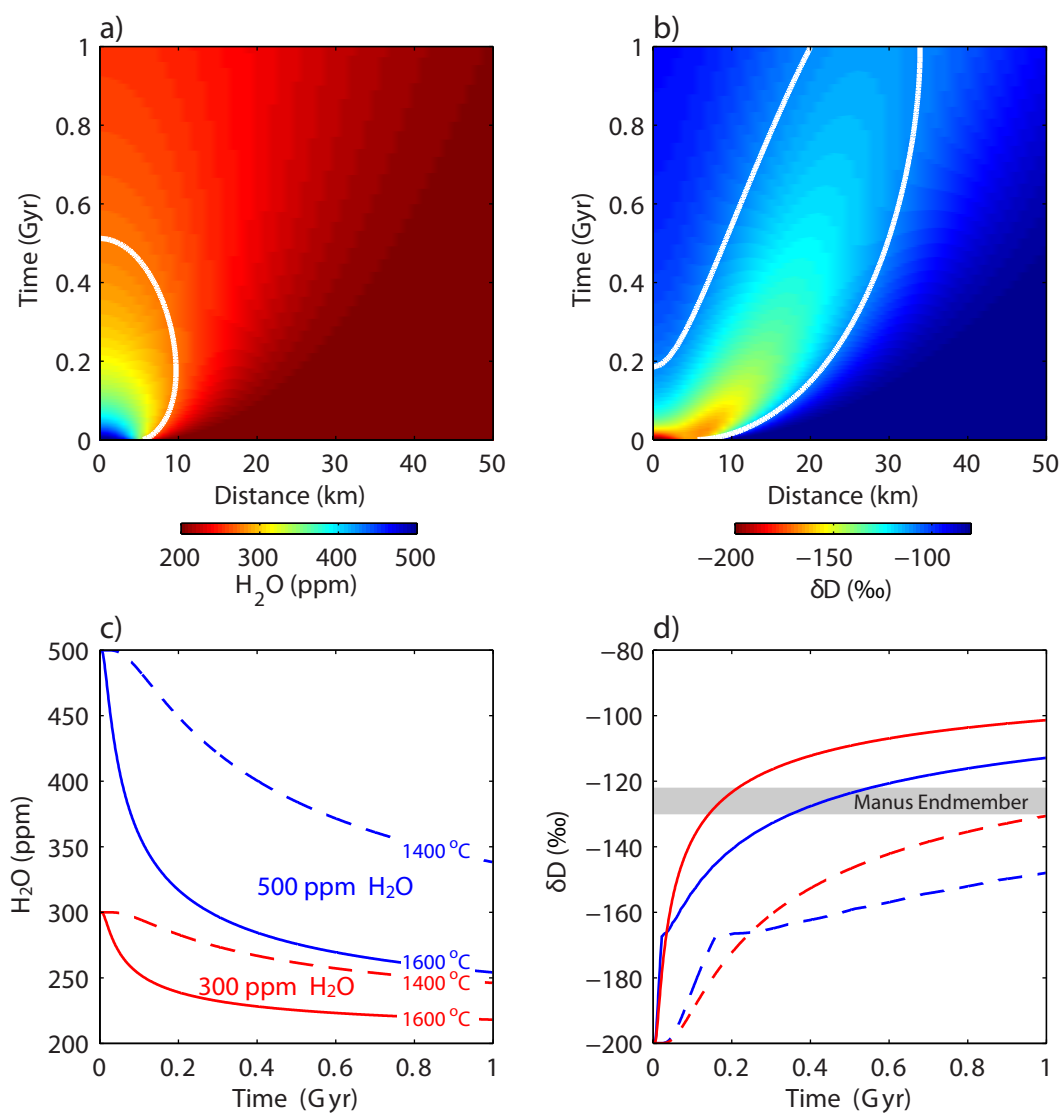


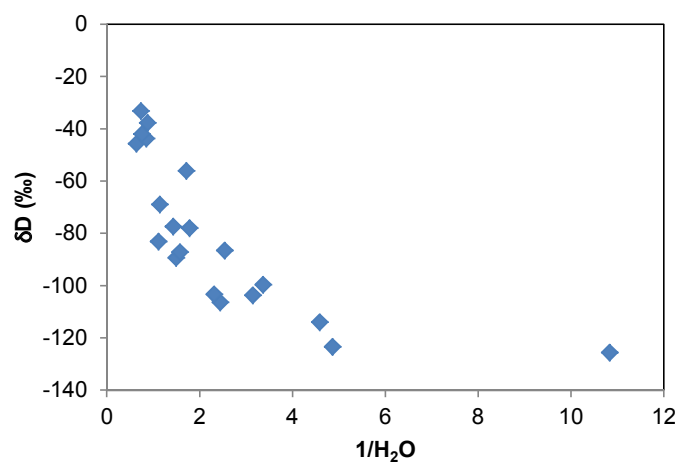
Figure 3

Table 1. Major volatile, trace element, δD , $\delta^{11}B$ and $^3He/^4He$ data for Manus Basin glasses

sample ^a	H ₂ O ^b (wt%)	CO ₂ (ppm)	F (ppm)	S (ppm)	Cl (ppm)	δD^c (‰)	$\delta^{11}B^d$ (‰)	H ₂ O/Ce ^e	Ba/La	$^3He/^4He^f$ (R/R _A)	$\delta^{18}O^f$ (‰)	$\delta^{13}C^g$ (‰)
BABB												
19-12	1.58	8	132	593	305	-46	2.4 ± 0.4	3257	16.2	3.42	6.14	
21-2	1.36	24	128	741	565	-33	5.8 ± 0.7	3665	19.3	8.83	5.93	-15.9
28-1	0.88	71	160	1212	402	-69	-0.6 ± 1.3	1710	9.9	11.98	5.75	-9.5
31-8	1.14	27	61	440	242	-38		3894	11.9	8.87	5.67	
33-1	0.56	67	122	1136	190	-78	-1.4 ± 1.2	1281	8.2	12.12	5.82	
34-1	0.59	67	121	1136	192	-56		1437	7.8	12.05	5.53	-6.8
40-6	1.18	12	182	920	1261	-44	-0.5 ± 0.9	1924	11.7	11.50		-8.9
41-3	1.33	14	151	875	1659	-42		2813	8.8	11.58	5.72	-16.1
MORB												
23-2	0.09	98	58	568	43	-126	-9.2 ± 2.1	367	1.8	15.14	5.28	-4.5
31-1	0.67	119	232	1376	201	-89	-5.3 ± 1.1	702	5.6	10.34		-9
32-5	0.22	149	136	1048	108	-114		512	3.6	13.48	5.48	-4.6
33-3	0.21	121	122	1088	94	-123		520	3.0	12.74	5.53	-5.6
36-2	0.30	167	116	945	160	-100	-6.7 ± 0.9	709	4.8	11.65	5.76	-6
38-3	0.41	178	178	1391	156	-106	-7.4 ± 0.7	693	4.6	12.71	5.51	-5.5
39-1	0.32	119	146	1214	116	-104	-10.8 ± 1.0	650	4.6	12.68	5.37	-6.5
42-1	0.70	95	185	1493	592	-77		1069	5.9	11.75	5.68	-8.1
43-1	0.90	65	285	1639	857	-83		947	5.9	11.59	5.8	-11.3
44-1	0.43	142	157	1309	278	-103	-3.1 ± 1.0	903	5.0	12.05	5.69	
45-1	0.39	111	179	1370	166	-86		665	4.7	12.56	5.5	-7.6
47-1	0.64	90	268	1718	699	-87		723	4.6	12.25	5.53	-10.3
arc												
14-5	1.37	6	529	80	2317			1509	48.8	1.02	6.03	
16-14	1.58	5	345	86	2116			2018	36.4		5.99	-33.2
17-1	1.48	5	727	34	3826		5.2 ± 0.4	1169	37.3	0.61	5.97	-28.3

^a Petrogenetic types are from Sinton et al. (2003)^b All volatiles are measured by ion probe and analytical uncertainties are 10%, as in Hauri (2002)^c Analytical uncertainty for δD measurements are ± 4 ‰, based on reproducibility of standards and the calibration curve^d B isotopes measured on WHOI's 1280 ion microprobe, errors reported at the 2 σ level^e Trace element analyses, measured by ion probe are included in supplementary documents^f Data from Macpherson et al. (1999) and Macpherson et al. (2000)^g Data from Shaw et al. (2004)

Long-term preservation of slab signatures in the mantle inferred from hydrogen isotopes



Supplementary Figure 1. δD versus $1/H_2O$. We note that all data with the exception of one sample (23-2) lie on a linear trend. This linear relationship is consistent with a mixing process rather than a degassing process.

Long-term preservation of slab signatures in the mantle inferred from hydrogen isoto

Supplementary Table 1. Sample details: type, location, and eruption depth

Sample	Type ^a	Site ^b	Lat. (S)	Long. (E)	Depth ^c (m)
MORB-1					
32-5	B	ETZ	3°25.2'	149°00.9'	2300-2420
33-3	B	ETZ	3°31.7'	149°28.7'	2090-2115
36-2	B	MSC	3°26.8'	149°57.8'	2155-2165
38-3	B	MSC	3°19.9'	150°04.9'	2200-2225
39-1	B	MSC	3°17.4'	150°07.7'	2285-2370
MORB seamount					
23-2	B	Smt	3°52.4'	149°58.0'	1390-1865
E-MORB					
31-1	B	ETZ	3°30.1'	149°15.5'	2075-2245
MORB-2					
42-1	B	MSC	3°09.6'	150°17.1'	2480-2490
43-1	B	MSC	3°08.0'	150°19.3'	2510-2545
44-1	B	MSC	3°05.2'	150°23.7'	2600-2630
45-1	B	MSC	3°03.9'	150°27.3'	2570-2670
46-2	B	MSC	3°02.0'	150°30.4'	2510-2560
47-1	B	MSC	3°04.6'	150°33.8'	2525-2580
BABB					
28-1	B	ETZ	3°39.4'	149°40.4'	2370-2440
31-8	B	ETZ	3°30.1'	149°15.5'	2075-2245
34-1	B	ETZ	3°36.4'	149°43.9'	2445-2510
40-6	B	MSC	3°14.9'	150°07.7'	2300-2310
41-3	BA	MSC	3°12.0'	150°12.5'	2375-2400
19-12	BA	SR	3°45.1'	151°09.5'	2625-2635
21-2	B	SR	3°50.4'	150°30.1'	2400-2465
Arc type					
14-5	A	EMR	3°42.9'	152°10.4'	1755-1950
16-14	BA	EMR	3°42.1'	151°52.4'	1980-2065
17-1	D	EMR	3°44.4'	151°38.8'	1685-1860

a. B-basalt, BA-basaltic andesite, A-andesite, D-dacite

b. ETZ-Extensional transform zone, MSC-Manus spreading centre, Smt-Seamount, SR-Southern

Long-term preservation of slab signatures in the mantle inferred from hydrogen is

Supplementary Table 2. Major and trace element analyses of Manus Basin glasses

	19-12	21-2	28-1	31-8	23-2	31-1	32-5	33-1
SiO₂	53.7	50.9	50.9	51.7	47.6	50.2	49.6	50.5
TiO₂	1.00	0.66	1.08	0.37	0.65	1.54	1.00	0.91
Al₂O₃	14.8	16.4	14.7	16.0	17.3	14.3	14.8	14.5
FeO	10.6	8.3	10.7	7.3	9.4	11.7	10.4	10.5
MnO	0.16	0.17	0.18	0.13	0.16	0.20	0.19	0.18
MgO	5.0	7.8	6.9	8.7	9.2	6.7	7.8	7.2
CaO	9.5	12.6	11.7	13.8	12.9	11.6	12.5	12.3
Na₂O	2.7	2.1	2.3	1.5	2.1	2.7	2.2	2.2
K₂O	0.24	0.21	0.15	0.08	0.03	0.13	0.06	0.09
P₂O₅	0.10	0.06	0.09	0.06	0.03	0.13	0.08	0.06
Li	4.9	2.6	3.6	2.2	2.4	4.0	3.4	3.3
Be	0.26	0.19	0.27	0.09	0.14	0.49	0.24	0.22
B	5.68	3.21	2.41	2.22	1.05	2.58	1.42	2.43
P	475	374	431	205	137	637	341	333
K	1465	1352	896	452	78	912	249	523
Sc	32.1	36.4	39.8	35.8	46.9	42.1	40.6	40.6
Ti	5006	3654	5938	1942	3759	8519	5637	4993
Cr	34	260	239	286	308	106	223	194
Sr	76	171	80	67	55	91	60	81
Y	21.3	15.0	24.9	9.2	22.7	32.1	23.1	20.8
Zr	17.2	10.2	18.0	5.3	11.5	29.8	16.2	14.3
Nb	0.60	0.28	0.92	0.45	0.18	3.24	0.66	0.59
Ba	27.9	27.5	16.0	12.9	1.2	18.1	4.5	11.4
La	1.7	1.4	1.6	1.1	0.6	3.2	1.3	1.4
Ce	4.9	3.7	5.1	2.9	2.5	9.6	4.3	4.4
Nd	3.7	4.0	5.1	2.0	3.2	8.5	5.2	4.9
Sm	1.5	1.5	1.7	0.7	1.6	2.6	3.6	1.5
Eu	1.6	1.3	1.8	0.9	2.5	2.6	1.2	1.6
Gd	1.9	1.5	2.5	0.9	2.3	3.7	2.3	2.0
Dy	2.6	2.3	3.2	1.2	2.6	4.3	3.3	2.6
Er	2.0	1.4	2.4	1.0	2.1	2.9	2.1	1.9
Yb	1.7	1.1	1.9	0.8	2.0	2.5	1.7	1.6
Hf	1.4	0.8	1.4	0.5	1.0	2.2	1.0	1.0
Pb	1.5	1.7	1.3	0.6	1.1	1.6	0.5	1.3
Th	0.11	0.07	0.11	0.08	0.03	0.14	0.03	0.08
U	0.09	0.05	0.03	0.04	0.02	0.04	0.02	0.03

Major element analyses are reported in wt% and trace element analyses are reported in

sotopes

33-3	34-1	36-2	38-3	39-1	40-6	41-1	41-3	42-1
50.6	51.1	50.4	51.0	50.9	51.9	68.4	52.4	50.9
1.02	0.91	0.92	1.37	1.23	1.07	0.81	0.93	1.32
14.2	14.7	14.8	13.6	13.8	15.0	11.4	15.1	13.8
11.3	10.5	10.0	12.9	12.2	10.7	9.5	9.7	12.5
0.21	0.18	0.18	0.24	0.21	0.19	0.17	0.16	0.22
7.5	7.3	8.2	6.6	7.0	6.0	0.6	6.4	6.1
12.4	12.4	12.5	11.0	11.5	10.9	4.5	11.2	10.6
2.4	2.3	2.2	2.5	2.4	2.7	2.8	2.5	2.6
0.05	0.08	0.06	0.07	0.06	0.21	0.33	0.13	0.10
0.07	0.06	0.05	0.09	0.08	0.10	0.21	0.09	0.07
3.4	3.2	2.9	4.4	4.1	3.8	14.8	3.1	4.2
0.24	0.21	0.22	0.31	0.28	0.31	0.99	0.24	0.32
1.20	1.87	1.52	1.63	1.75	2.86	4.61	1.64	2.08
308	326	321	470	396	504	662	385	502
196	519	329	383	325	1294	2157	732	519
43.8	40.3	40.3	43.1	41.4	36.7	17.1	35.7	41.3
5750	5013	5192	7597	6560	5761	3283	5000	7287
122	196	307	107	97	67	4	113	53
57	83	57	61	58	129	57	120	76
25.0	21.5	21.2	32.4	27.0	24.2	79.7	19.4	29.9
16.2	13.7	15.2	23.7	18.9	19.1	85.8	14.7	22.8
0.59	0.50	0.92	1.05	0.77	0.79	3.03	0.63	0.99
3.2	11.1	6.0	7.6	5.9	26.0	36.7	14.4	12.2
1.1	1.4	1.2	1.7	1.3	2.2	5.7	1.6	2.1
4.0	4.1	4.2	5.9	4.9	6.2	18.1	4.7	6.5
5.0	4.6	4.6	6.6	5.6	5.8	21.1	4.6	6.1
2.0	1.6	2.0	2.5	2.0	1.8	6.3	1.3	2.5
1.8	1.6	1.7	2.1	1.8	1.9	4.8	1.3	2.4
2.4	2.0	2.2	3.3	4.3	2.5	7.7	2.0	2.8
3.5	2.6	2.7	4.2	3.4	3.6	9.8	2.5	4.0
2.3	1.9	2.1	4.1	2.4	2.0	7.0	1.4	2.6
2.1	3.5	1.9	2.6	2.1	2.0	6.6	1.5	2.5
1.4	1.1	1.2	1.8	1.7	1.4	5.8	1.2	1.6
2.2	1.6	0.8	1.5	1.0	1.3	1.8	0.7	1.1
0.07	0.06	0.48	0.08	0.07	0.12	0.27	0.07	0.07
0.02	0.05	0.02	0.03	0.03	0.08	0.10	0.04	0.08

1 ppm

43-1	44-1	45-1	47-1	14-5	16-14	17-1
52.5	50.8	51.6	51.6	64.0	54.5	64.4
1.76	1.18	1.39	1.80	0.82	0.59	0.79
13.0	13.8	13.7	13.1	14.5	15.4	16.1
14.7	12.1	13.1	15.1	7.3	7.9	5.4
0.22	0.22	0.21	0.24	0.15	0.12	0.11
4.7	6.8	6.4	5.5	1.8	5.4	1.2
9.1	11.3	11.2	9.8	5.1	9.8	5.0
3.0	2.4	2.5	2.8	3.4	2.7	3.8
0.14	0.06	0.07	0.11	1.14	0.84	1.36
0.16	0.08	0.11	0.15	0.24	0.17	0.29
6.3	4.0	4.6	6.3	6.6	3.7	9.0
0.48	0.27	0.32	0.49	0.57	0.40	0.70
2.48	1.68	1.88	2.37	20.88	12.17	16.23
702	404	478	718	826	710	1042
805	345	396	675	7071	5593	10845
39.6	41.9	42.0	40.5	18.9	28.3	16.6
9459	6630	7618	10118	3248	2933	3787
22	84	51	53	6	46	6
70	60	60	69	325	308	185
43.5	28.0	31.4	44.8	13.6	10.6	19.4
35.8	19.4	23.0	34.6	16.6	13.5	23.8
1.65	0.87	1.00	1.54	0.64	0.59	1.05
17.0	6.8	7.8	12.8	191.6	128.3	193.3
2.9	1.4	1.7	2.8	3.9	3.5	5.2
9.5	4.8	5.9	8.8	9.1	7.8	12.7
9.4	5.9	6.5	9.2	7.9	5.9	8.8
3.3	2.3	2.4	3.3	1.8	1.4	2.3
2.9	2.2	2.2	2.9	3.3	2.2	3.7
4.5	2.5	2.9	4.4	1.7	1.5	2.3
6.2	3.7	4.2	5.7	1.9	1.5	2.4
3.9	2.9	3.0	3.9	1.2	1.2	1.8
3.6	2.1	2.5	3.5	1.1	0.8	1.6
2.5	1.4	1.5	6.6	1.1	0.9	1.6
1.5	1.1	1.1	1.9	2.1	1.8	1.7
0.10	0.06	0.09	0.11	0.27	0.29	0.42
0.03	0.01	0.10	0.05	0.21	0.18	0.30